4-2018

Readily Accessible Shape-Memory Effect in a Porous Interpenetrated Coordination Network

Mohana Shivanna
University of Limerick

Qing-Yuan Yang
University of Limerick

Alankriti Bajpai
University of Limerick

Susan Sen
Kyoto University

Nobuhiko Hosono
Kyoto University

See next page for additional authors

MATERIALS SCIENCE

Readily accessible shape-memory effect in a porous interpenetrated coordination network

Mohana Shivanna,[1]* Qing-Yuan Yang,[1]* Alankriti Bajpai,[1] Susan Sen,[2] Nobuhiko Hosono,[2] Shinpei Kusaka,[2] Tony Pham,[3] Katherine A. Forrest,[3] Brian Space,[3] Susumu Kitagawa,[2†] Michael J. Zaworotko[1†]

Shape-memory effects are quite well-studied in general, but there is only one reported example in the context of porous materials. We report the second example of a porous coordination network that exhibits a sorbate-induced shape-memory effect and the first in which multiple sorbates, N_2, CO_2 and CO promote this effect. The material, a new threefold interpenetrated pcu network, $[Zn_2(4,4'\text{-biphenyldicarboxylate})_2(1,4\text{-bis}(4\text{-pyridyl})\text{benzene})]_n$ (X-pcu-3-Zn-3i), exhibits three distinct phases: the as-synthesized α phase; a denser-activated β phase; and a shape-memory γ phase, which is intermediate in density between the α and β phases. The γ phase is kinetically stable over multiple adsorption/desorption cycles and only reverts to the β phase when heated at >400 K under vacuum. The α phase can be regenerated by soaking the γ phase in *N*,*N*′-dimethylformamide. Single-crystal x-ray crystallography studies of all three phases provide insight into the shape-memory phenomenon by revealing the nature of interactions between interpenetrated networks. The β and γ phases were further investigated by in situ coincidence powder x-ray diffraction, and their sorption isotherms were replicated by density functional theory calculations. Analysis of the structural information concerning the three phases of X-pcu-3-Zn-3i enabled us to understand structure-function relationships and propose crystal engineering principles for the design of more examples of shape-memory porous materials.

INTRODUCTION

A shape-memory effect occurs when the morphology of a material changes in response to an external stimulus, and the new morphology is persistent until another stimulus is applied. Shape-memory effects are well-recognized in general (*1*, *2*) but remain rare in the context of porous materials. Metal-organic materials (MOMs) (*3*, *4*), also known as porous coordination polymers (*5*, *6*) or metal-organic frameworks (MOFs) (*7*, *8*), are a subclass of porous materials that are extraordinarily diverse in composition owing to their modularity and amenability to design from first principles (*9*). There are at least 20,000 porous MOMs, and ca. 150 of these MOMs are known to exhibit structural flexibility, in some cases, extreme structural flexibility (*10*, *11*). Flexibility occurs in response to external stimuli, such as guest incorporation/removal, temperature, pressure, or light (*12*–*16*). The origins of flexibility are well-studied and attributed to flexible MOMs (FMOMs) being able to exhibit one or more of the following phenomena: (i) changes in metal-ligand coordination geometry (*17*, *18*); (ii) cleavage and regeneration of coordination bonds (*19*); and (iii) distortion/contortion of organic linker(s) (*20*, *21*). Dynamic behavior is also known in zeolites, but it tends to be less pronounced (*22*, *23*). The fact that FMOMs can exhibit breathing or swelling suggests that they might be amenable to shape-memory effects (table S1). However, most of the FMOMs reported to date undergo reversible structural changes in response to interfacial sorbate/sorbent interactions, albeit with hysteresis (*20*, *24*, *25*). To our knowledge, the only example of an FMOM that exhibits a shape-memory effect, $[Cu_2(bdc)_2(bpy)]_n$, does not return to its activated form upon MeOH solvation/desolvation. Rather, it reverts to the original phase upon heating at 473 K, and the shape-memory effect is particle size–dependent (*26*). Therefore, whereas shape-memory effects are well-documented in metal alloys (*27*, *28*), polymers (*29*, *30*), and ceramics (*31*), it remains a rare and poorly understood phenomenon in crystalline porous materials.

Here, we report the second observation of a shape-memory effect in FMOMs through the study of gas adsorption in an expanded variant of $[Cu_2(bdc)_2(bpy)]_n$ and $[Zn_2(L1)(L2)_2]_n$ (**X-pcu-3-Zn-3i**), both of which can be regarded as derivatives of DMOF-1 (*32*, *33*) and its analogs (*34*–*37*). The shape-memory effect exhibited by **X-pcu-3-Zn-3i** was recognized by distinctive sorption isotherms characteristic of shape-memory porous materials (Fig. 1) and occurs under the influence of N_2, CO_2, or CO (Fig. 2). A suite of experiments involving single-crystal x-ray diffraction (XRD), gas sorption, in situ variable temperature/pressure powder XRD (PXRD), and molecular modeling were performed to afford insight into the shape-memory behavior of **X-pcu-3-Zn-3i**.

RESULTS AND DISCUSSION

Single crystals of the as-synthesized **X-pcu-3-Zn-3i** and **X-pcu-3-Zn-3i-α** were isolated by solvothermal reaction of ligands **L1** [1,4-bis(4-pyridyl)benzene] and **L2** (4,4′-biphenyldicarboxylic acid) with $Zn(NO_3)_2{\cdot}6H_2O$ in *N*,*N*′-dimethylformamide (DMF) at 120°C for 24 hours. The extended ligand (X ligand) **L1** was prepared by following our previously reported procedure (*38*), whereas **L2** was purchased from Sigma-Aldrich and used as received. The crystal structure of **X-pcu-3-Zn-3i-α** was determined by single-crystal XRD (SCXRD) and exhibits the triclinic space group *P*-1 (table S2). Dinuclear Zn "paddlewheel" molecular building blocks (MBBs) (*3*) are linked equatorially by dicarboxylate dianions to form distorted square lattice (**sql**) networks. The axial sites of the paddlewheel MBBs are coordinated by dipyridyl linkers (**L1**), which cross-link the **sql** networks to generate three-dimensional (3D) networks with primitive cubic (**pcu**) topology (Fig. 2). Three independent **pcu** networks interpenetrate (fig. S1), yet **X-pcu-3-Zn-3i-α** still exhibits 46% guest accessible volume occupied by solvent DMF molecules and a density without solvent of 1.046 g/cm^3.

[1]Department of Chemical Sciences, Bernal Institute, University of Limerick, Limerick, Republic of Ireland. [2]Institute for Integrated Cell-Material Sciences (WPI-iCeMS), Kyoto University, Yoshida, Sakyo-ku, Kyoto 606-8501, Japan. [3]Department of Chemistry, University of South Florida, 4202 East Fowler Avenue, Tampa, FL 33620, USA.
*These authors contributed equally to this work.
†Corresponding author. Email: kitagawa@icems.kyoto-u.ac.jp (S.K.); michael.zaworotko@ul.ie (M.J.Z.)

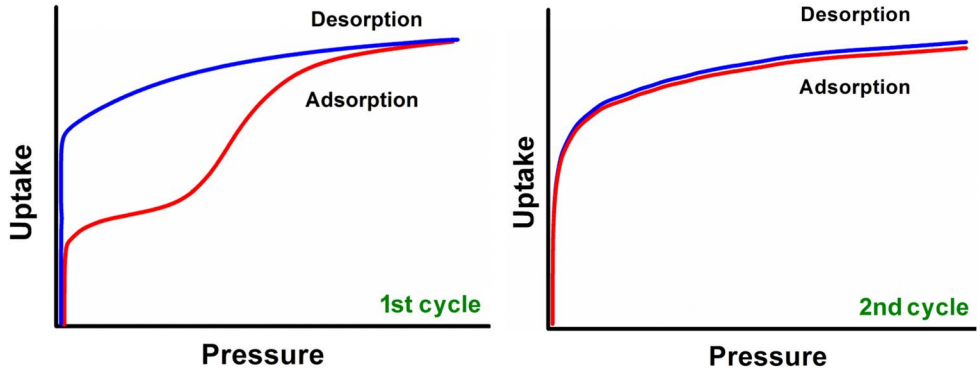

Fig. 1. The typical sorption isotherms associated with a shape-memory effect in an FMOM. The first adsorption cycle occurs in step(s), whereas desorption lacks any steps (left). The second and subsequent sorption cycles are examples of type I isotherms (right).

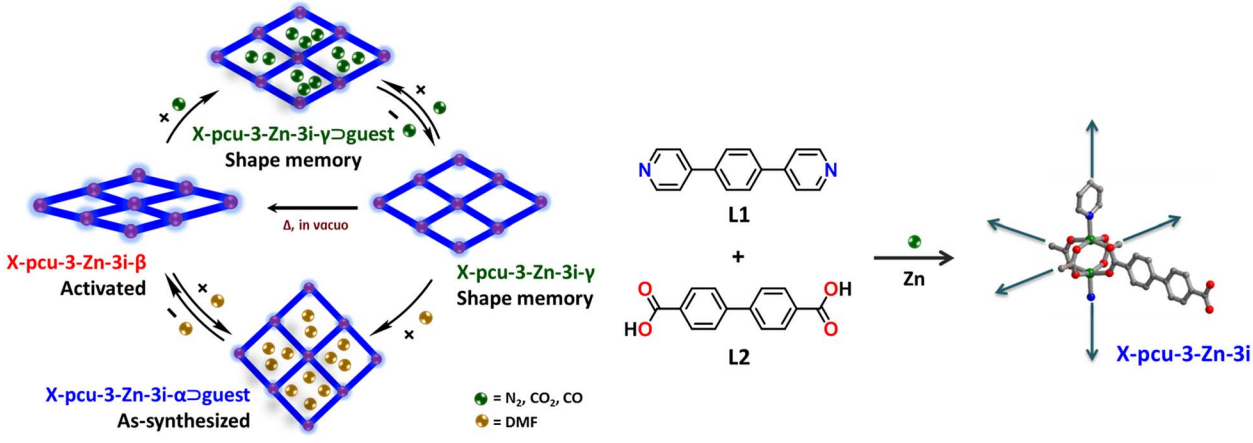

Fig. 2. Structure of X-pcu-3-Zn and its phase changes under external stimuli. A schematic illustration of the shape-memory effect in **X-pcu-3-Zn-3i** (left). The structure of **X-pcu-3-Zn-3i** is composed of axially coordinated **L1** linkers that cross-link 2D square grids to form a 3D structure (right).

Single crystals of **X-pcu-3-Zn-3i-β** were obtained from as-synthesized crystals of **X-pcu-3-Zn-3i-α** by heating at 130°C under vacuum for 12 hours. **X-pcu-3-Zn-3i-β** also exists in the triclinic space group *P*-1 and its density is 1.333 g/cm^3. Comparison of the crystal structures of **X-pcu-3-Zn-3i-α** and **X-pcu-3-Zn-3i-β** reveals that the **pcu** networks in **X-pcu-3-Zn-3i-β** are distorted, reducing the guest accessible volume from 46 to 15% (Fig. 2). The phase transformation between **X-pcu-3-Zn-3i-α** and **X-pcu-3-Zn-3i-β** was also studied by in situ variable temperature PXRD, which revealed that transformation at 120°C is complete within 10 min (figs. S2 and S6). Those phase transformations in FMOMs can occur in single-crystal–to–single-crystal (SC-SC) fashion as has been previously observed for FMOMs (*39*, *40*).

Gas sorption and in situ coincidence PXRD measurements

The gas adsorption performance of **X-pcu-3-Zn-3i-β** was studied for N_2 (77 K), CO (82 K), and CO_2 (195 K). Activation was conducted by washing as-synthesized **X-pcu-3-Zn-3i-**α with DMF followed by heating at 130°C under vacuum for 12 hours. Two distinct steps were observed in the CO_2 adsorption isotherm at 195 K (fig. S3): a plateau at 0.2 to 0.3 bar with uptake of 65 g/cm^3 followed by a second step leading to uptake of 160 g/cm^3 at 1 bar. The desorption isotherm does not match the adsorption isotherm; it exhibits no step and large hysteresis (fig. S3). We attribute the stepped adsorption isotherm to a structural transformation from **X-pcu-3-Zn-3i-β** to a new phase, **X-pcu-3-Zn-3i-γ**, as verified by PXRD (fig. S8). Notably, **X-pcu-3-Zn-3i-γ** does not revert to **X-pcu-3-Zn-3i-β** under vacuum but, after being subjected to heating at 130°C in vacuo for 2 hours, it once again exhibits the stepped isotherm of **X-pcu-3-Zn-3i-β** (fig. S4). The structure of **X-pcu-3-Zn-3i-γ** was determined by SCXRD (monoclinic space group *C*2/*c*, density of 1.117 g/cm^3; table S2), and the calculated PXRD pattern for **X-pcu-3-Zn-3i-γ** matches that of the experimental PXRD pattern. **X-pcu-3-Zn-3i-γ** exhibits 34% guest accessible volume. These results are indicative of a shape-memory effect in **X-pcu-3-Zn-3i**.

To validate the shape-memory effect in **X-pcu-3-Zn-3i**, in situ coincidence PXRD was performed using CO_2 at 195 K; diffraction patterns were recorded at adsorption/desorption points a to f (Fig. 3). The PXRD pattern at point d (0.9 bar CO_2) reveals that transformation from **X-pcu-3-Zn-3i-β** to **X-pcu-3-Zn-3i-γ** had been induced by CO_2. From point d to f (desorption), there is no change in the PXRD pattern, which corresponds to the calculated PXRD of **X-pcu-3-Zn-3i-γ**. **X-pcu-3-Zn-3i-γ** reverts to **X-pcu-3-Zn-3i-β** after heating at 130°C under vacuum in situ for 2 hours (Fig. 3, left). In situ coincidence PXRD measurements were also performed using N_2 (77 K) and CO (82 K); PXRD patterns were recorded at adsorption/desorption points. Sorption isotherms characteristic of the shape-memory effect observed for CO_2 at 195 K were obtained but there are multiple steps in both the N_2 and CO adsorption isotherms. This is plausible because N_2 and CO offer weaker interfacial interactions than CO_2, enabling the observation of

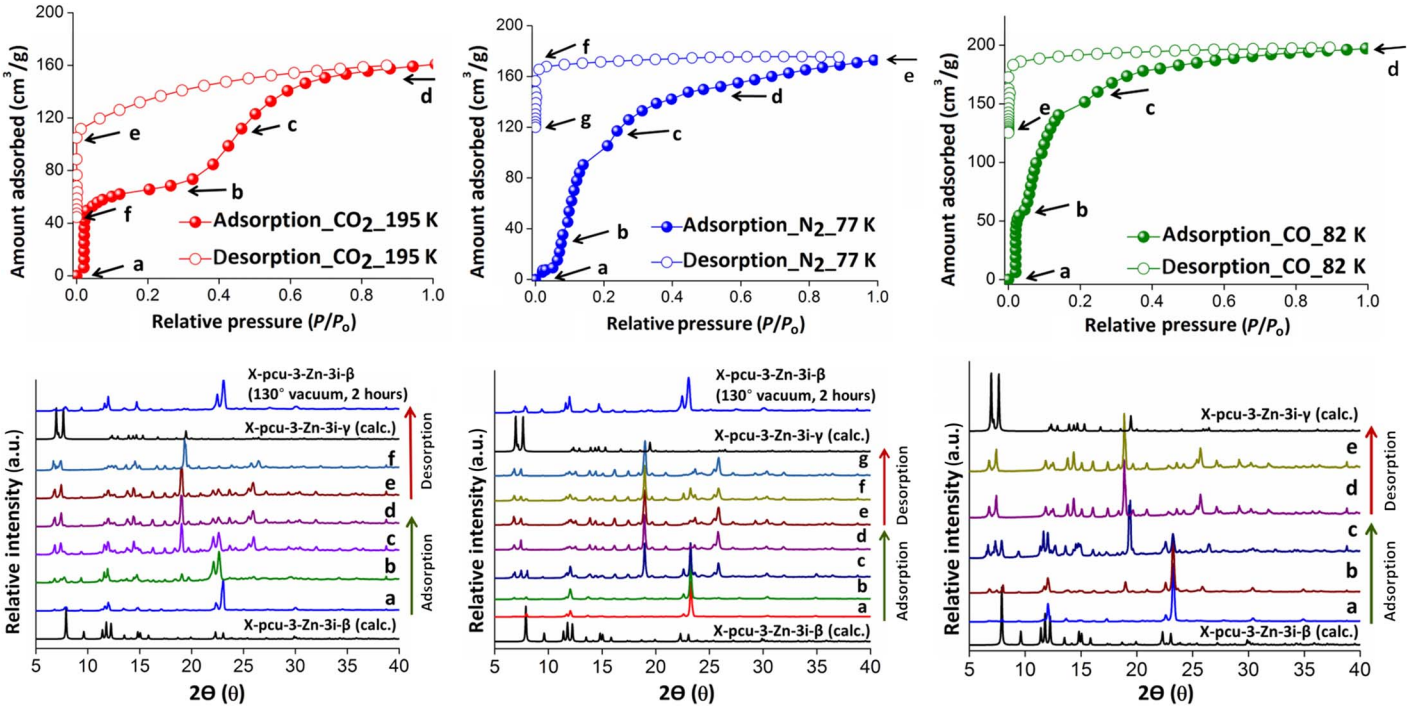

Fig. 3. In situ coincidence PXRD measurements. PXRD patterns for **X-pcu-3-Zn-3i** are correlated with adsorption and desorption isotherms for CO_2 at 195 K (left), N_2 at 77 K (middle), and CO at 82 K (right). a.u., arbitrary unit.

intermediate phases. For N_2 sorption (Fig. 3, middle), there is little uptake at low pressure (0.05 bar, 9 g/cm^3); however, at 0.14 bar N_2, there is a step (to 90 g/cm^3) before a second step occurs at point c. These steps are indicative of a narrow- to large-pore phase transformation involving at least two large-pore phases. The PXRD patterns at points d and e reveal that transformation to **X-pcu-3-Zn-3i-γ** had been induced by N_2. From points e to g (desorption), there is no change in the PXRD pattern, but **X-pcu-3-Zn-3i-γ** reverts to **X-pcu-3-Zn-3i-β** after heating at 130°C under vacuum for 2 hours (Fig. 3, middle). In the case of CO sorption (Fig. 3, right), there are also steps at points a, b, and c, which are consistent with narrow- to large-pore phase transformation to **X-pcu-3-Zn-3i-γ**.

Furthermore, 10 consecutive cycles of CO_2 sorption at 195 K were performed (Fig. 4, left). The first cycle exhibits a stepped isotherm, whereas subsequent cycles are type I isotherms with uptake of ca. 170 g/cm^3 (Fig. 4, left). High-pressure CO_2 adsorption at 298 K also reveals a stepped isotherm with gate opening at 15 bar and, once again, the desorption isotherm exhibits no step and a large hysteresis loop (Fig. 4, right). Consecutive cycles measured at other temperatures (298, 288, and 305 K) all exhibit type I isotherms (fig. S5). The PXRD pattern of a sample isolated after these experiments matches the calculated PXRD of **X-pcu-3-Zn-3i-γ** (fig. S8). **X-pcu-3-Zn-3i-γ** fails to revert to **X-pcu-3-Zn-3i-β** upon heating up to 240°C (fig. S10) but reverts to **X-pcu-3-Zn-3i-α** by soaking in DMF (5 min) but not with methanol, acetonitrile, or dichloromethane (2 days; fig. S9). These results indicate that the new shape-memory phase reported here, **X-pcu-3-Zn-3i-γ**, can be accessed with multiple sorbates and that it is kinetically stable over a range of temperatures, sorbates, and pressures.

Modeling studies

The sorption profiles were modeled using the single-crystal structures of **X-pcu-3-Zn-3i-β** and **X-pcu-3-Zn-3i-γ**. The simulated CO_2 isotherms at 195 K for **X-pcu-3-Zn-3i-β** and **X-pcu-3-Zn-3i-γ** are in good agreement with the corresponding experimental isotherm (fig. S15); below 0.3 bar, the experimental isotherm matches the simulated isotherm for **X-pcu-3-Zn-3i-β**. The uptake from the simulated isotherm of **X-pcu-3-Zn-3i-γ** is comparable to its experimental uptake (fig. S15).

Structural insight into shape memory

To gain insight into the origins of the shape-memory phenomenon, we analyzed and compared the crystal structures of **X-pcu-3-Zn-3i-α**, **X-pcu-3-Zn-3i-β**, and **X-pcu-3-Zn-3i-γ**. In **X-pcu-3-Zn-3i-α**, the paddlewheel MBBs are slightly distorted ($\angle_{\text{linker-MBB-linker}}$ = 70.9° to 109.6°) and **L2** linkers align out of plane with respect to each other (fig. S11). There exist π···π [$D_{C\cdots C}$ = 3.547 (5) and 3.518(5) Å] interactions between the interpenetrated networks, but there are no intermolecular interactions between blue and green networks (Fig. 5, left bottom). In **X-pcu-3-Zn-3i-β**, the paddlewheel MBB is highly distorted ($\angle_{\text{linker-MBB-linker}}$ = 46.8° to 132.2°) and **L2** linkers align out of plane with respect to each other (fig. S12). Being the densest phase, the interpenetrated networks are in close proximity as evidenced C–H···O [$D_{C\cdots O}$ = 3.587(6) Å] and π···π [$D_{C\cdots C}$ = 3.710(6) Å] interactions (Fig. 5, middle bottom). In **X-pcu-3-Zn-3i-γ**, the paddlewheel MBB is slightly distorted ($\angle_{\text{linker-MBB-linker}}$ = 61.1° to 117.7°) and **L2** linkers align in-plane with respect to each other (fig. S13). The interpenetrated networks exhibit C–H···O interactions [$D_{C\cdots O}$ = 3.289(5) and 3.446(4) Å; Fig. 5, right bottom]. Structural transformation between the three phases can be attributed to sliding of the interpenetrated networks (fig. S1), a previously observed phenomenon (*13*).

CONCLUSIONS

X-pcu-3-Zn-3i is only the second example of a porous material that exhibits a shape-memory effect and the first in which multiple sorbates induce such an effect. The shape-memory phase (**X-pcu-3-Zn-3i-γ**) was

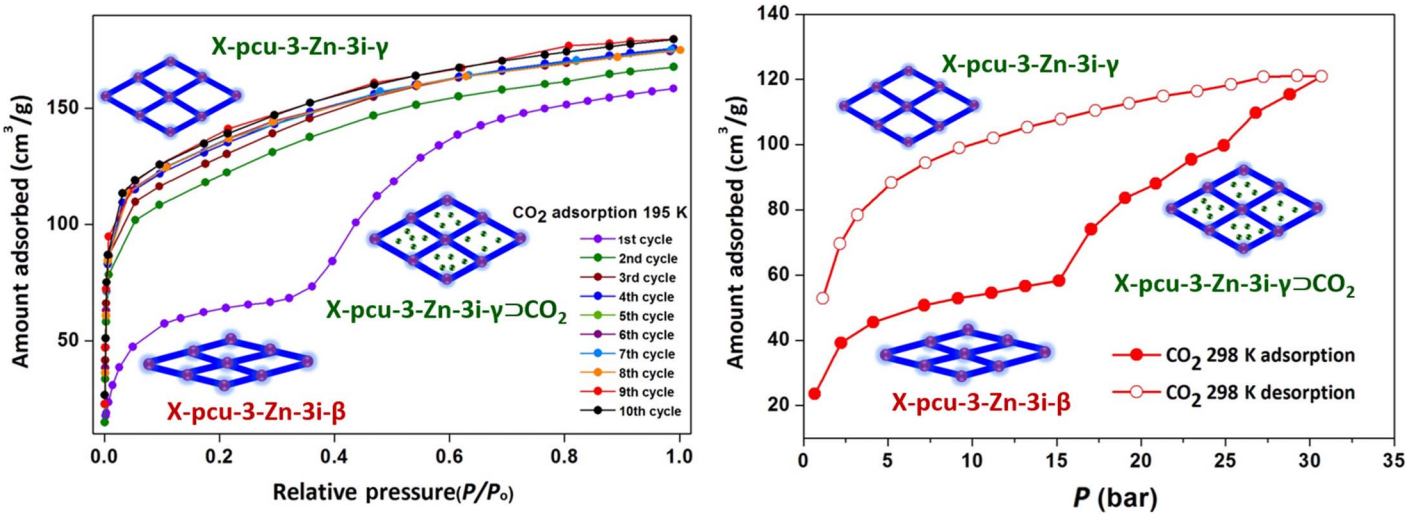

Fig. 4. Low- and high-pressure CO_2 sorption on X-pcu-3-Zn. Ten consecutive cycles of CO_2 sorption at 195 K (left). First cycle of high-pressure CO_2 at 298 K (right).

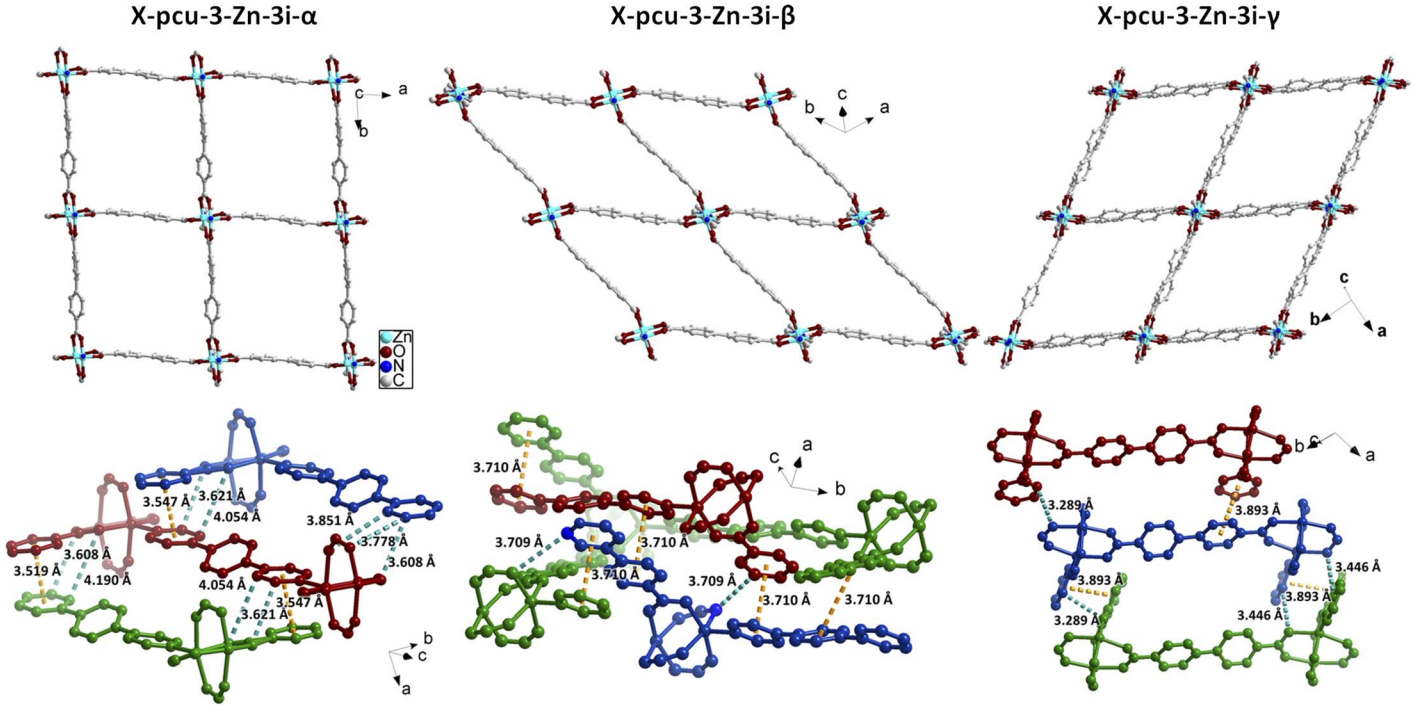

Fig. 5. Structural insights for the three phases. The **sql** networks of the α, β, and γ forms of **X-pcu-3-Zn-3i** (top) and how three of these networks (red, green, and blue, respectively) interact through C–H···O (teal) and π···π (yellow) interactions (bottom).

observed to be accessible under the influence of several stimuli (CO_2 at 195 K, N_2 at 77 K, CO at 82 K, and high-pressure CO_2 at 298 K) and is kinetically stable over a range of pressures, temperature, and sorbates. The following factors would intuitively be expected to facilitate a kinetically stable shape-memory FMOM, and all three are observed for **X-pcu-3-Zn-3i**: (i) framework flexibility induced by sorbent-sorbate interfacial interactions and extended ligands (X ligands) that can distort more readily than shorter ligands; (ii) interpenetration that enables framework-framework interactions to stabilize less dense variants; and (iii) reduced strain in the MBBs and linkers when in the shape-memory phase. As noted by a reviewer, it is possible that existing FMOMs are as yet unrecognized as shape-memory porous materials. It is a characteristic feature of FMOMs that they exhibit "stepped" or "S-shaped" isotherm profiles, but this does not prove or even suggest a shape-memory effect, which can only be identified by measurement of multiple cycles of adsorption/desorption. We have analyzed the isotherms for all reported FMOMs (ca. 130 materials), and 10 of these materials (table S1) exhibit strong hysteresis that could be consistent with a shape-memory effect. However, we do not know whether any of these materials are recyclable, regardless of whether they exhibit

the features listed above to sustain a shape-memory phase. **X-pcu-3-Zn-3i** is highly modular and amenable to fine-tuning of the ligands and the metal centers. **X-pcu-3-Zn-3i** is therefore a platform to determine whether the three factors listed above are crystal engineering principles for the design of families of shape-memory porous materials.

MATERIALS AND METHODS

Synthesis of [Zn_2(4,4′-biphenyldicarboxylate)$_2$(1,4-bis(4-pyridyl)benzene)]$_n$·6DMF (X-pcu-3-Zn-3i-α)

Commercially available reagents were purchased in high-purity grade and used as received. A mixture of $Zn(NO_3)_2{\cdot}6H_2O$ (14.8 mg, 0.05 mmol; purchased from Sigma-Aldrich), **L1** (7.7 mg, 0.025 mmol; prepared as previously reported), and **L2** (12.11 mg, 0.05 mmol; purchased from Sigma-Aldrich) were dissolved in DMF (3 ml) in a 14-ml glass vial. The vial was capped tightly and placed in an oven at 120°C. Colorless block-shaped crystals were isolated after 24 hours. The contents were cooled to room temperature, filtered, and washed with DMF (3 ml × 10 ml) to afford 60% yield of **X-pcu-3-Zn-3i**-α (based on **L1** as the limiting reagent).

Preparation of [Zn_2(L2)$_2$(L1)]·DMF (X-pcu-3-Zn-3i-β)

Crystals of the **X-pcu-3-Zn-3i-β** were prepared by heating **X-pcu-3-Zn-3i-α** at 130°C under vacuum for 12 hours.

Preparation of [Zn_2(L2)$_2$(L1)] (X-pcu-3-Zn-3i-γ)

Shape-memory phase **X-pcu-3-Zn-3i-γ** was obtained by gas sorption of first cycle at CO_2 at 195 K of **X-pcu-3-Zn-3i-β** phase.

In situ variable temperature PXRD, PXRD and SCXRD experiments

PXRD experiments were conducted using a PANalytical Empyrean diffractometer equipped with a PIXcel3D detector operating in scanning line detector mode with an active length of 4 using 255 channels. The diffractometer was outfitted with an Empyrean Cu LFF (long fine-focus) HR tube (9430 033 7310x), operated at 40 kV and 40 mA and Cu Kα radiation (λα = 1.540598 Å). Incident beam optics included the Fixed Divergence slit with anti-scatter slit PreFIX module, with a 1/8° divergence slit and a 1/4° anti-scatter slit, a 10-mm fixed incident beam mask and a Soller slit (0.04 rad). Divergent beam optics included a P7.5 anti-scatter slit, a Soller slit (0.04 rad), and a Ni β filter. In a typical experiment, data were collected via a continuous scan in the range of 5° to 45° (2θ) with a step size of 0.02° at a scan rate of 0.1° min^{-1}. Raw data were then evaluated using the X'Pert HighScore Plus software v4.1 (PANalytical). In situ variable temperature PXRD was collected under N_2 atmosphere by increasing the temperature to 10°C/10 min; water cooling system was adopted to control the temperature. SCXRD data were collected on a Bruker Quest diffractometer equipped with a complementary metal-oxide semiconductor detector and IμS microfocus x-ray source (Cu Kα, λ = 1.5418 Å). Absorption corrections were applied by using the multiscan program SADABS. Structural solution and refinement against Fobs data were carried out using the SHELXL programs.

Coincident PXRD/adsorption measurement

Coincident PXRD/adsorption measurements were measured on a Rigaku SmartLab with Cu Kα radiation (Rigaku) connected to a BELSORP-18PLUS volumetric adsorption equipment (MicrotracBEL Corp.) and synchronized with each other. To control the temperature, the adsorption equipment was connected to a cryostat. We started with the as-synthesized MOM, **X-pcu-3-Zn-3i-α**, of known weight. The sample was placed on a copper plate and activated under high vacuum (at a pressure around 200 Pa) at 130°C for 12 hours. The weight of the evacuated sample (~70 mg) was determined under inert atmosphere and set on a cryostat system for in situ evacuation under high vacuum (<10 to 2 Pa) at 393 K for 2 hours before the experiments. CO_2 adsorption was carried out by setting the temperature of the cryostat at the measurement temperature (195 K) followed by controlled introduction of CO_2 gas to the sample cell. The degree of the adsorption was determined by the decrease in the gas introduction pressure at the equilibrium state. The PXRD pattern of the sample containing adsorbate was simultaneously measured at each equilibrium point of the adsorption isotherms.

In situ SC-SC XRD

In situ SC-SC was studied by selecting a single crystal, which was glued to a glass fiber and inserted into a glass capillary with a wall thickness of 0.01 mm and an outer diameter of 0.2 mm. The crystal was maintained at 300 K, and SCXRD data were collected (**X-pcu-3-Zn-3i**-α). SCXRD data were then collected at 323, 363, and 403 K for approximately 4 hours at each temperature. The unit cell parameters at each temperature were calculated.

SUPPLEMENTARY MATERIALS

Supplementary material for this article is available at http://advances.sciencemag.org/cgi/content/full/4/4/eaaq1636/DC1

fig. S1. Structure of the three phases.
fig. S2. Diffraction pattern and single-crystal images.
fig. S3. Low-pressure gas sorption.
fig. S4. Recyclability of shape-memory phase at 195 K CO_2.
fig. S5. High-pressure CO_2 sorption.
fig. S6. In situ variable temperature PXRD.
fig. S7. Solvent-induced phase change.
fig. S8. PXRD data for **X-pcu-3-Zn-3i-γ** obtained from different experiments.
fig. S9. Phase change from γ to α phase.
fig. S10. Variable temperature PXRD of shape-memory phase.
fig. S11. Distortion of paddlewheel MBB and orientation of X-ligands in **X-pcu-3-Zn-3i-α**.
fig. S12. Distortion of paddlewheel MBB and orientation of X ligands in **X-pcu-3-Zn-3i-β**.
fig. S13. Distortion of paddlewheel MBB and orientation of X ligands in **X-pcu-3-Zn-3i-γ**.
fig. S14. Thermogravimetric analysis (TGA) profiles.
fig. S15. Comparison of modeling and experimental isotherm.
fig. S16. Free-energy difference.
fig. S17. Chemically distinct atoms in **X-pcu-3-Zn-3i-α**.
fig. S18. The chemically distinct atoms in **X-pcu-3-Zn-3i-β**.
fig. S19. The chemically distinct atoms in **X-pcu-3-Zn-3i-γ**.
table S1. Examples of previously reported FMOMs with large hysteresis.
table S2. Crystal data and refinement parameters.
table S3. Numerical labeling of atoms corresponds to fig. S17.
table S4. The crystallographic distances (in Å) between various atoms in **X-pcu-3-Zn-3i-α**.
table S5. The partial charges (in e^-) for the chemically distinct atoms in **X-pcu-3-Zn-3i-β**.
table S6. The crystallographic distances (in Å) between various atoms in **X-pcu-3-Zn-3i-β**.
table S7. Numerical labeling of atoms corresponds to fig. S18.
table S8. Labels of atoms correspond to fig. S18.
table S9. Calculated energies for three phases.
References (*41*–*62*)

REFERENCES AND NOTES

1. K. Otsuka, C. M. Wayman, *Shape memory materials* (Cambridge Univ. Press, 1998).
2. M. Behl, M. Y. Razzaq, A. Lendlein, Multifunctional shape-memory polymers. *Adv. Mater.* **22**, 3388–3410 (2010).
3. J. J. Perry IV, J. A. Perman, M. J. Zaworotko, Design and synthesis of metal–organic frameworks using metal–organic polyhedra as supermolecular building blocks. *Chem. Soc. Rev.* **38**, 1400–1417 (2009).

4. T. R. Cook, Y.-R. Zheng, P. J. Stang, Metal–organic frameworks and self-assembled supramolecular coordination complexes: Comparing and contrasting the design, synthesis, and functionality of metal–organic materials. *Chem. Rev.* **113**, 734–777 (2013).
5. S. Kitagawa, R. Kitaura, S.-i. Noro, Functional porous coordination polymers. *Angew. Chem. Int. Ed. Engl.* **43**, 2334–2375 (2004).
6. S. R. Batten, S. M. Neville, D. R. Turner, *Coordination Polymers: Design, Analysis and Application Introduction* (RSC Publishing, 2009).
7. M. Schroder, *Functional Metal–Organic Frameworks: Gas Storage, Separation and Catalysis* (Springer-Verlag, 2009).
8. L. R. MacGillivray, C. M. Lukehart, *Metal–Organic Framework Materials* (Wiley, 2014).
9. B. Moulton, M. J. Zaworotko, From molecules to crystal engineering: Supramolecular isomerism and polymorphism in network solids. *Chem. Rev.* **101**, 1629–1658 (2001).
10. C. Serre, C. Mellot-Draznieks, S. Surblé, N. Audebrand, Y. Filinchuk, G. Férey, Role of solvent-host interactions that lead to very large swelling of hybrid frameworks. *Science* **315**, 1828–1831 (2007).
11. Y.-S. Wei, K.-J. Chen, P.-Q. Liao, B.-Y. Zhu, R.-B. Lin, H.-L. Zhou, B.-Y. Wang, W. Xue, J.-P. Zhang, X.-M. Chen, Turning on the flexibility of isoreticular porous coordination frameworks for drastically tunable framework breathing and thermal expansion. *Chem. Sci.* **4**, 1539–1546 (2013).
12. S. Horike, S. Shimomura, S. Kitagawa, Soft porous crystals. *Nat. Chem.* **1**, 695–704 (2009).
13. A. Schneemann, V. Bon, I. Schwedler, I. Senkovska, S. Kaskel, R. A. Fischer, Flexible metal–organic frameworks. *Chem. Soc. Rev.* **43**, 6062–6096 (2014).
14. E. R. Engel, A. Jouaiti, C. X. Bezuidenhout, M. W. Hosseini, L. J. Barbour, Activation-dependent breathing in a flexible metal–organic framework and the effects of repeated sorption/desorption cycling. *Angew. Chem. Int. Ed. Engl.* **56**, 8874–8878 (2017).
15. E. J. Carrington, C. A. McAnally, A. J. Fletcher, S. P. Thompson, M. Warren, L. Brammer, Solvent-switchable continuous-breathing behaviour in a diamondoid metal–organic framework and its influence on CO_2 versus CH_4 selectivity. *Nat. Chem.* **9**, 882–889 (2017).
16. G. Férey, C. Serre, Large breathing effects in three-dimensional porous hybrid matter: Facts, analyses, rules and consequences. *Chem. Soc. Rev.* **38**, 1380–1399 (2009).
17. P. K. Thallapally, J. Tian, M. Radha Kishan, C. A. Fernandez, S. J. Dalgarno, P. B. McGrail, J. E. Warren, J. L. Atwood, Flexible (breathing) interpenetrated metal–organic frameworks for CO_2 separation applications. *J. Am. Chem. Soc.* **130**, 16842–16843 (2008).
18. K. L. Mulfort, O. K. Farha, C. D. Malliakas, M. G. Kanatzidis, J. T. Hupp, An interpenetrated framework material with hysteretic CO_2 uptake. *Chemistry* **16**, 276–281 (2010).
19. G. K. Kole, J. J. Vittal, Solid-state reactivity and structural transformations involving coordination polymers. *Chem. Soc. Rev.* **42**, 1755–1775 (2013).
20. C. Serre, F. Millange, C. Thouvenot, M. Noguès, G. Marsolier, D. Louër, G. Férey, Very large breathing effect in the first nanoporous chromium(III)-based solids: MIL-53 or $Cr^{III}(OH)\{O_2C–C_6H_4–CO_2\}\{HO_2C–C_6H_4–CO_2H\}_x·H_2O_y$. *J. Am. Chem. Soc.* **124**, 13519–13526 (2002).
21. J. Seo, C. Bonneau, R. Matsuda, M. Takata, S. Kitagawa, Soft secondary building unit: Dynamic bond rearrangement on multinuclear core of porous coordination polymers in gas media. *J. Am. Chem. Soc.* **133**, 9005–9013 (2011).
22. C. A. Fyfe, G. J. Kennedy, C. T. De Schutter, G. T. Kokotailo, Sorbate-induced structural-changes in ZSM-5 (silicalite). *J. Chem. Soc. Chem. Commun.* **8**, 541–542 (1984).
23. A. Sartbaeva, S. A. Wells, M. M. J. Treacy, M. F. Thorpe, The flexibility window in zeolites. *Nat. Mater.* **5**, 962–965 (2006).
24. S. Yang, X. Lin, W. Lewis, M. Suyetin, E. Bichoutskaia, J. E. Parker, C. C. Tang, D. R. Allan, P. J. Rizkallah, P. Hubberstey, N. R. Champness, K. M. Thomas, A. J. Blake, M. Schröder, A partially interpenetrated metal–organic framework for selective hysteretic sorption of carbon dioxide. *Nat. Mater.* **11**, 710–716 (2012).
25. J. A. Mason, J. Oktawiec, M. K. Taylor, M. R. Hudson, J. Rodriguez, J. E. Bachman, M. I. Gonzalez, A. Cervellino, A. Guagliardi, C. M. Brown, P. L. Llewellyn, N. Masciocchi, J. R. Long, Methane storage in flexible metal–organic frameworks with intrinsic thermal management. *Nature* **527**, 357–361 (2015).
26. Y. Sakata, S. Furukawa, M. Kondo, K. Hirai, N. Horike, Y. Takashima, H. Uehara, N. Louvain, M. Meilikhov, T. Tsuruoka, S. Isoda, W. Kosaka, O. Sakata, S. Kitagawa, Shape-memory nanopores induced in coordination frameworks by crystal downsizing. *Science* **339**, 193–196 (2013).
27. Y.-D. Wang, Y. Ren, H. Li, H. Choo, M. L. Benson, D. W. Brown, P. K. Liaw, L. Zuo, G. Wang, D. E. Brown, E. E. Alp, Tracing memory in polycrystalline ferromagnetic shape-memory alloys. *Adv. Mater.* **18**, 2392–2396 (2006).
28. Y. Tanaka, Y. Himuro, R. Kainuma, , Y. Sutou, T. Omori, K. Ishida, Ferrous polycrystalline shape-memory alloy showing huge superelasticity. *Science* **327**, 1488–1490 (2010).
29. A. Lendlein, H. Jiang, O. Jünger, R. Langer, Light-induced shape-memory polymers. *Nature* **434**, 879–882 (2005).
30. T. Xie, Tunable polymer multi–shape memory effect. *Nature* **464**, 267–270 (2010).
31. A. Lai, Z. Du, C. L. Gan, C. A. Schuh, Shape memory and superelastic ceramics at small scales. *Science* **341**, 1505–1508 (2013).
32. K. Seki, S. Takamizawa, W. Mori, Design and gas adsorption property of a three-dimensional coordination polymer with a stable and highly porous framework. *Chem. Lett.* **30**, 332–333 (2001).
33. D. N. Dybtsev, H. Chun, K. Kim, Rigid and flexible: A highly porous metal–organic framework with unusual guest-dependent dynamic behavior. *Angew. Chem. Ger. Edit.* **116**, 5143–5146 (2004).
34. B. Chen, C. Liang, J. Yang, D. S. Contreras, Y. L. Clancy, E. B. Lobkovsky, O. M. Yaghi, S. Dai, A microporous metal–organic framework for gas-chromatographic separation of alkanes. *Angew. Chem. Int. Ed. Engl.* **45**, 1390–1393 (2006).
35. B. Chen, S. Ma, E. J. Hurtado, E. B. Lobkovsky, H.-C. Zhou, A triply interpenetrated microporous metal–organic framework for selective sorption of gas molecules. *Inorg. Chem.* **46**, 8490–8492 (2007).
36. O. K. Farha, J. T. Hupp, Rational design, synthesis, purification, and activation of metal–organic framework materials. *Acc. Chem. Res.* **43**, 1166–1175 (2010).
37. P. Kanoo, R. Haldar, S. K. Reddy, A. Hazra, S. Bonakala, R. Matsuda, S. Kitagawa, S. Balasubramanian, T. K. Maji, Crystal dynamics in multi-stimuli-responsive entangled metal–organic frameworks. *Chemistry* **22**, 15864–15873 (2016).
38. A. Bajpai, H. S. Scott, T. Pham, K.-J. Chen, B. Space, M. Lusi, M. L. Perry, M. J. Zaworotko, Towards an understanding of the propensity for crystalline hydrate formation by molecular compounds. *IUCrJ* **3**, 430–439 (2016).
39. J.-P. Zhang, Y.-Y. Lin, W.-X. Zhang, X.-M. Chen, Temperature- or guest-induced drastic single-crystal-to-single-crystal transformations of a nanoporous coordination polymer. *J. Am. Chem. Soc.* **127**, 14162–14163 (2005).
40. H. Aggarwal, P. M. Bhatt, C. X. Bezuidenhout, L. J. Barbour, Direct evidence for single-crystal to single-crystal switching of degree of interpenetration in a metal–organic framework. *J. Am. Chem. Soc.* **136**, 3776–3779 (2014).
41. J. Lincke, D. Lässig, J. Moellmer, C. Reichenbach, A. Puls, A. Moeller, R. Gläser, G. Kalies, R. Staudt, H. Krautscheid, A novel copper-based MOF material: Synthesis, characterization and adsorption studies. *Microporous Mesoporous Mater.* **142**, 62–69 (2011).
42. H.-R. Fu, J. Zhang, Structural transformation and hysteretic sorption of light hydrocarbons in a flexible Zn-pyrazole-adenine framework. *Chemistry* **21**, 5700–5703 (2015).
43. B. Fernandez, G. Beobide, I. Sánchez, F. Carrasco-Marín, J. M. Seco, A. J. Calahorro, J. Cepeda, A. Rodríguez-Diéguez, Controlling interpenetration for tuning porosity and luminescence properties of flexible MOFs based on biphenyl-4,4′-dicarboxylic acid. *CrstEngComm* **18**, 1282–1294 (2016).
44. R. Haldar, S. K. Reddy, V. M. Suresh, S. Mohapatra, S. Balasubramanian, T. K. Maji , Flexible and rigid amine-functionalized microporous frameworks based on different secondary building units: Supramolecular isomerism, selective CO_2 capture, and catalysis. *Chemistry* **20**, 4347–4356 (2014).
45. P. Kanoo, R. Sambhu, T. K. Maji, Guest-specific double- or single-step adsorption in a flexible porous framework based on a mixed-ligand system. *Inorg. Chem.* **50**, 400–402 (2011).
46. X. Li, X. Chen, F. Jiang, L. Chen, S. Lu, Q. Chen, M. Wu, D. Yuan, M. Hong, The dynamic response of a flexible indium based metal–organic framework to gas sorption. *Chem. Commun.* **52**, 2277–2280 (2016).
47. W.-P. Wu, Z.-S. Li, B. Liu, P. Liu, Z.-P. Xi, Y.-Y. Wang, Double-step CO_2 sorption and guest-induced single-crystal-to-single-crystal transformation in a flexible porous framework. *Dalton Trans.* **44**, 10141–10145 (2015).
48. P. Kanoo, R. Matsuda, R. Kitaura, S. Kitagawa, T. K. Maji, Topological difference in 2D layers steers the formation of rigid and flexible 3D supramolecular isomers: Impact on the adsorption properties. *Inorg. Chem.* **51**, 9141–9143 (2012).
49. S. Yang, L. Liu, J. Sun, K. M. Thomas, A. J. Davies, M. W. George, A. J. Blake, A. H. Hill, A. N. Fitch, C. C. Tang, M. Schröder, Irreversible network transformation in a dynamic porous host catalyzed by sulfur dioxide. *J. Am. Chem. Soc.* **135**, 4954–4957 (2013).
50. N. Metropolis, A. W. Rosenbluth, M. N. Rosenbluth, A. H. Teller, E. Teller, Equation of state calculations by fast computing machines. *J. Chem. Phys.* **21**, 1087–1092 (1953).
51. A. L. Mullen, T. Pham, K. A. Forrest, C. R. Cioce, K. McLaughlin, B. Space, A polarizable and transferable PHAST CO_2 potential for materials simulation. *J. Chem. Theory Comput.* **9**, 5421–5429 (2013).
52. J. Applequist, J. R. Carl, K.-K. Fung, Atom dipole interaction model for molecular polarizability. Application to polyatomic molecules and determination of atom polarizabilities. *J. Am. Chem. Soc.* **94**, 2952–2960 (1972).
53. D.-Y. Peng, D. B. Robinson, A new two-constant equation of state. *Ind. Eng. Chem. Fundamen.* **15**, 59–64 (1976).
54. W. L. Jorgensen, D. S. Maxwell, J. Tirado-Rives, Development and testing of the OPLS all-atom force field on conformational energetics and properties of organic liquids. *J. Am. Chem. Soc.* **118**, 11225–11236 (1996).
55. A. K. Rappe, C. J. Casewit, K. S. Colwell, W. A. Goddard III, W. M. Skiff, UFF, a full periodic table force field for molecular mechanics and molecular dynamics simulations. *J. Am. Chem. Soc.* **114**, 10024–10035 (1992).
56. W. J. Stevens, H. Basch, M. Krauss, Compact effective potentials and efficient shared-exponent basis-sets for the first- and second-row atoms. *J. Chem. Phys.* **81**, 6026–6033 (1984).
57. M. Valiev, E. J. Bylaska, N. Govind, K. Kowalski, T. P. Straatsma, H. J. J. Van Dam, D. Wang, J. Nieplocha, E. Apra, T. L. Windus, W. A. de Jong, NWChem: A comprehensive and

scalable open-source solution for large scale molecular simulations. *Comput. Phys. Commun.* **181**, 1477–1489 (2010).
58. L. E. Chirlian, M. M. Francl, Atomic charges derived from electrostatic potentials: A detailed study. *J. Comput. Chem.* **8**, 894–905 (1987).
59. P. Th. van Duijnen, M. Swart, Molecular and atomic polarizabilities: Thole's model revisited. *J. Phys. Chem. A* **102**, 2399–2407 (1998).
60. K. A. Forrest, T. Pham, A. Hogan, K. McLaughlin, B. Tudor, P. Nugent, S. D. Burd, A. Mullen, C. R. Cioce, L. Wojtas, M. J. Zaworotko, B. Space, Computational studies of CO_2 sorption and separation in an ultramicroporous metal–organic material. *J. Phys. Chem. C* **117**, 17687–17698 (2013).
61. G. Kresse, J. Furthmüller, Efficient iterative schemes for ab initio total-energy calculations using a plane-wave basis set. *Phys. Rev. B* **54**, 11169–11186 (1996).
62. G. Kresse, D. Joubert, From ultrasoft pseudopotentials to the projector augmented-wave method. *Phys. Rev. B* **59**, 1758–1775 (1999).

Acknowledgments: Coincident PXRD/adsorption measurements were performed in Kyoto University. **Funding:** This work was supported by the Science Foundation Ireland (award 13/RP/B2549). B.S. acknowledges the NSF (award no. CHE-1152362), including support from the Major Research Instrumentation Program (award no. CHE-1531590), the computational resources that were made available by a XSEDE Grant (no. TG-DMR090028), and the use of the services provided by Research Computing at the University of South Florida. N.H. and S. Kitagawa acknowledge the financial support of KAKENHI, Grant-in-Aid for Specially Promoted Research (no. 25000007) from the Japan Society of the Promotion of Science. S. Kusaka and S. Kitagawa thank JST ACCEL, Japan (grant no. JPMJAC1302).
Author contributions: M.J.Z. and M.S. conceived the experiments and designed the study. M.S. conducted the material synthesis and measurements. M.S. and Q.-Y.Y. characterized the phases reported herein (SCXRD, PXRD, and low- and high-pressure gas sorption). A.B. developed the synthetic method to prepare **L1**. S.S., N.H., and S. Kusaka conducted the in situ coincidence PXRD measurements. T.P., K.A.F., and B.S. conducted the modeling experiments. M.J.Z., S. Kitagawa, Q.-Y.Y., A.B., and M.S. wrote the manuscript. All authors contributed to the interpretation of the data and discussion. **Competing interests:** The authors declare that they have no competing interests. **Data materials and availability:** All data needed to evaluate the conclusions in the paper are present in the paper and/or the Supplementary Materials. Crystallographic data for this manuscript have been deposited at the Cambridge Crystallographic Data Centre under deposition numbers CCDC 1565491 and 1565493. Additional data related to this paper may be requested from M.J.Z. (Michael.Zaworotko@ul.ie).

Submitted 18 October 2017
Accepted 12 March 2018
Published 27 April 2018
10.1126/sciadv.aaq1636

Citation: M. Shivanna, Q.-Y. Yang, A. Bajpai, S. Sen, N. Hosono, S. Kusaka, T. Pham, K. A. Forrest, B. Space, S. Kitagawa, M. J. Zaworotko, Readily accessible shape-memory effect in a porous interpenetrated coordination network. *Sci. Adv.* **4**, eaaq1636 (2018).

Science Advances

Readily accessible shape-memory effect in a porous interpenetrated coordination network

Mohana Shivanna, Qing-Yuan Yang, Alankriti Bajpai, Susan Sen, Nobuhiko Hosono, Shinpei Kusaka, Tony Pham, Katherine A. Forrest, Brian Space, Susumu Kitagawa and Michael J. Zaworotko

Sci Adv **4** (4), eaaq1636.
DOI: 10.1126/sciadv.aaq1636